Catalysis Today 427 (2024) 114437

Contents lists available at ScienceDirect

Catalysis Today

journal homepage: www.elsevier.com/locate/cattod

Propane dehydrogenation over Pt and Ga-containing MFI zeolites with modified acidity and textural properties

Adriana S. Oliveira [a,b], Jennifer Cueto [a], María del Mar Alonso-Doncel [a], Martin Kubů [c], Jiří Čejka [c], David P. Serrano [a,d], Rafael A. García-Muñoz [d,*]

[a] Thermochemical Processes Unit, IMDEA Energy Institute, Avda. Ramón de la Sagra, 3, Móstoles, Madrid, Spain
[b] Department of Chemical Engineering, Faculty of Science, Autonomous University of Madrid, Ciudad Universitaria de Cantoblanco, Madrid, Spain
[c] Department of Physical and Macromolecular Chemistry, Faculty of Science, Charles University, Hlavova 8, Prague, Czech Republic
[d] Chemical and Environmental Engineering Group, Rey Juan Carlos University. C/ Tulipán s/n, Móstoles, Madrid, Spain

ARTICLE INFO

Keywords:
Propane dehydrogenation
Pt catalyst
Ga-MFI catalyst
Stability

ABSTRACT

A variety of oxides (titanium, tin, calcium, magnesium, and gallium) were supported over nano-crystalline ZSM-5 zeolite (n-ZSM-5) by wet impregnation, characterized and evaluated for propane dehydrogenation (PDH) reaction. To enhance the catalytic performance of the oxide-modified n-ZSM-5, Pt nanoparticles were also dispersed over the oxides-supported zeolite catalysts by wet impregnation. Finally, Ga-containing MFI zeolites were used as catalysts in the PDH. Ga was incorporated into the zeolite by two different methods, via hydrothermal synthesis and via wet impregnation. In the PDH reaction, Pt-containing samples exhibited a high initial catalytic activity although they suffered a fast deactivation by coke deposition. On the contrary, Ga-containing MFI catalysts showed a remarkable stability in the PDH reaction. In particular, the catalyst in which Ga was incorporated into the MFI structure by hydrothermal synthesis (Ga-MFI (nSH)) achieved the highest catalytic performance in PDH (9% conversion and 80% propylene selectivity) due to the synergy between the Brønsted and Lewis acid sites (BAS and LAS) and the optimal strength of its LAS sites. These results denote the great potential of Ga-MFI zeolites as catalysts in PDH reactions.

1. Introduction

Propylene is a highly demanded chemical building block to produce a wide range of high-value chemicals, such as polypropylene, acrylonitrile, propylene oxide, acrylic acid, etc. [1,2]. The typical production of propylene relies on steam cracking and fluid catalytic cracking of naphtha and oils, but cracking processes are insufficient to meet the growing global demand. Accordingly, the catalytic propane dehydrogenation reaction is becoming an interesting alternative, especially taking into account the high propane availability from shale gas exploitation [3,4]. Thus, propane dehydrogenation (PDH) supplied 13.6 million metric tons of propylene in 2019, representing ~11% of worldwide propylene production [5].

Propane dehydrogenation (PDH) is a reaction strongly limited by its high endothermicity, requiring high reaction temperatures above 550 °C and low propane pressure to obtain suitable conversions [6]. However, these elevated temperatures can lead to undesired secondary reactions including cracking, aromatization and oligomerization reactions as a result of the higher reactivity of propylene relative to propane [7].

As the key parameter appears to be the scission of the of the C-H bond of propane, Cr- and Pt-based catalysts are widely used and implemented in commercial processes (e.g. the Catofin and Oleflex processes using chromium- and platinum-based catalysts, respectively) [6]. However, the Cr-based catalysts have a major drawback due to the low selectivity to propylene and a high deactivation rate as a consequence of the coke deposition on the surface, together with its environmental concern. In contrast, palladium- and platinum-based catalysts have shown excellent performance in PDH reactions due to their ability for selective activation of C-H bonds [4,8,9]. However, platinum species typically experience a decrease in the activity at the high temperatures required due to sintering by Otswald ripening. Various strategies have been reported to overcome these shortcomings. Linic et al. [10] reported outstanding results in PDH using catalysts based on silica-supported platinum-tin nanoparticles operating at thermodynamically limited conversion levels, with exceptional stability and high selectivity to propylene. Other very promising microporous supports are zeolites since Pt species

* Corresponding author.
E-mail address: rafael.garcia@urjc.es (R.A. García-Muñoz).

https://doi.org/10.1016/j.cattod.2023.114437
Received 14 July 2023; Received in revised form 10 October 2023; Accepted 22 October 2023
Available online 24 October 2023

confined within their micropores present enhanced stability against sintering even at high temperatures or pressures [11,12]. Thus, it is very important to properly choose the method of Pt incorporation to better define its location and the properties that will impart to the PDH reaction. Liu et al. [13] reported an approach based on the transformation of two-dimensional ITQ-1 into three-dimensional MCM-22, which allowed the incorporation of Pt single atoms and nanoclusters in the internal channels to provide the catalysts with exceptionally high thermal stability. Similarly, layers of IPC-1P were used to stabilize Pt nanoclusters by condensing the layers into PCR zeolite [14]. In subsequent research, Liu et al. [15] reported how the introduction of a moderate amount of K^+ in the MFI zeolite hydrothermal synthesis permits that Pt atoms were selectively dispersed in the sinusoidal 10-ring channels of the MFI zeolite, suppressing the sintering of Pt nanoclusters through a stabilization effect and being very effective in the PDH reaction.

However, low availability of Pt and its high cost make the search for alternative catalysts essential. In this context, catalysts based on metal oxides, such as vanadium oxides, zinc oxides and gallium oxides are being used as interesting alternatives in the PDH reaction, exhibiting lower toxicity and lower cost than Cr- and Pt-based catalysts [16,17]. Among them, gallium (Ga)-based catalysts are emerging as a promising alternative in the PDH process due to their dehydrogenation activity. Nevertheless, conventional gallium oxides-based materials also suffer from deactivation and promote cyclization and aromatization reactions to a great extension [18–20]. To overcome these negative effects, a variety of Ga-containing zeolite sites have been considered. In particular, Ga addition into MFI zeolites allows the modification of the strength and concentration of the different acid sites depending on whether the Ga is incorporated in the framework or is present in the form of extra-framework species, implying the formation of several types of Ga-sites able to activate the C-H bonds and, as a consequence, causing a variation in the distribution of the products of the PDH reaction [1,21–24].

However, although the catalytic activity of Ga-based catalysts in the PDH process has been extensively studied, further research is needed to explore the nature and location of the active sites, the influence of the Si/Ga ratio, the Brønsted and Lewis acid sites concentration, the character of the support and the method of incorporation of Ga species, etc., all to improve the catalytic performance, and increase both propane conversion and propylene selectivity.

In this work, a wide variety of catalysts, based on the zeolitic MFI structure, have been investigated in the propane dehydrogenation reaction. Metal oxide- and Pt-modified metal oxides n-ZSM-5 catalysts were prepared to evaluate the effect of their textural and acidic properties on the catalytic performance. On the other hand, with the aim of finding a new alternative to the costly and scarce Pt, Ga was introduced into MFI zeolitic materials by two different methods, via hydrothermal synthesis and via wet impregnation to investigate the effect of the location of Ga species and the concentration of acid sites on their catalytic performance.

The results evidenced a better catalytic activity of these materials in the PDH reaction, mainly the Ga-MFI (nanosheet (nSH)) zeolite, due to a synergistic combination of Brønsted and Lewis acid sites (BAS and LAS) together with a higher strength of the LAS sites. In addition, these materials also showed a higher stability than Pt-based catalysts. The results denote the potential of Ga MFI zeolites as catalysts in PDH reactions.

2. Experimental

2.1. Catalysts preparation

Several oxide-supported catalysts were prepared by wet impregnation method using n-ZSM-5 (nanocrystalline ZSM-5, Si/Al: 42, Clariant CZP90) as support and ethanol as solvent. These catalysts were prepared with 10 wt% of metal oxide loading, with the aim of modifying significantly the textural and acidity properties of the support. Magnesium (II) nitrate hexahydrate ($Mg(NO_3)_2{\cdot}6\ H_2O$, Fischer Scientific, 98%), calcium nitrate tetrahydrate ($Ca(NO_3)_2{\cdot}4\ H_2O$, Fischer Scientific), tin (II) chloride dihydrate ($SnCl_2{\cdot}2\ H_2O$, Sigma Aldrich, 98%) and titanium (IV) oxyacetylacetonate ($C_{10}H_{14}O_5Ti$, Sigma Aldrich, 90%) were used as precursor salts of the metal oxides. Impregnation was carried out at 60 ºC and 200 rpm for 6 h in two consecutive steps to achieve a better dispersion. In each step, 50% of the amount of metal oxide precursor required for the impregnation was used and the ratio of 1 g of support per 10 mL of solution was maintained. After each impregnation step, the solvent was removed on a rotary evaporator (50 ºC, 10 mbar) and the solid recovered was dried at 100 ºC overnight. Afterward, the prepared samples were calcined at 550 ºC for 4 h in air (heating rate of 1.8 ºC/min). The samples were designated as MgO-n-ZSM-5, CaO-n-ZSM-5, SnO_2-n-ZSM-5 and TiO_2-n-ZSM-5.

Pt-containing catalysts were also prepared by wet impregnation method using tetraammineplatinum (II) nitrate ($[Pt(NH_3)_4](NO_3)_2$, Sigma Aldrich, 99.995%) as metal precursor. The commercial n-ZSM-5 and also the materials previously prepared by incorporating metal oxides were used as supports. These catalysts were prepared using 0.5 wt% Pt loading to avoid the use of large quantities of this expensive and scarce material. The metal precursor was first dissolved in water and then the supports were added to this solution, using 1 g of support per 10 mL of solution. The solution was kept under stirring (200 rpm) at room temperature for 6 h and then the solvent was removed on a rotary evaporator (50 ºC, 10 mbar). The recovered solids were calcined at 500 ºC for 2 h in air (heating rate of 1.8 ºC/min) and reduced at 500 ºC for 2 h in H_2 (50 mL/min). The samples were denoted as Pt-n-ZSM-5, Pt-MgO-n-ZSM-5, Pt-CaO-n-ZSM-5, Pt-SnO_2-n-ZSM-5, and Pt-TiO_2-n-ZSM-5.

Regarding the Ga-containing catalysts, a framework Ga-containing zeolite, Ga-MFI (nanosheet (nSH)) zeolite was synthesized by hydrothermal method according to literature procedures [25] from a synthesis gel with the following composition: 100 SiO_2: 1.5 Ga_2O_3: 30 Na_2O: 10 SDA: 15 H_2SO_4: 3200 H_2O. Gallium (III) sulfate ($Ga_2(SO_4)_3$, Sigma Aldrich, 99.99%), water glass (SiO_2 = 26.5 wt%, Na_2O = 10.6 wt%, Sigma Aldrich), sodium hydroxide solution (NaOH, Merck, 50%), tetraethyl orthosilicate (TEOS, Sigma Aldrich, 99%,), sulfuric acid (H_2SO_4, Lachema, Czechia, 98%), 1-bromodocosane (TCI, 98%), N,N,N′, N′-tetramethyl-1,6-diaminohexane (TCI, 98%), toluene (Sigma Aldrich, 99.8%), acetonitrile (Merck, 99%), diethyl ether (Penta, Czech Republic), 1-bromohexane (Sigma Aldrich, 98%), ammonium nitrate (NH_4NO_3, Merck, 95%) were used as reactants during the synthesis and SDA preparation. Crystallization was performed in a Teflon-lined stainless-steel autoclave at 150 °C for 7 days. The final product was then filtered, dried overnight at 60 °C and calcined at 550 °C for 8 h in air. Finally, the sodium form was ion-exchanged into the proton form by treatment (4 times) with a 1.0 M ammonium nitrate solution for 4 h (using 1 g of zeolite per 100 mL of solution) followed by calcination at 450 °C for 5 h. On the other hand, for comparison Ga-n-ZSM-5 and Ga-Silicalite-1 catalysts were prepared by wet impregnation method, using the same and three times the Ga content of the Ga-MFI (nSH) catalyst. It should be emphasized that the Gallium present on the n-ZSM-5 and Silicalite-1 supports is in the Ga_2O_3 state, unlike the Ga-MFI sample, where Gallium is found within the zeolitic framework. Thus, the samples were denoted as 2.8% and 7.4% Ga-n-ZSM-5 and 2.8% Ga-Silicalite-1. The synthesis gel of the Silicalite-1 sample was prepared in a round bottom flask containing tetraethyl orthosilicate (TEOS, Aldrich, 98%), tetrapropylammonium hydroxide (TPAOH, Alfa-Aesar, 40% w/w aqueous solution) and deionized water in a molar concentration of 100 SiO_2: 18 TPAOH: 2500 H_2O. TEOS hydrolysis was performed under magnetic stirring for 40 h at room temperature. The ethanol produced was then removed by evaporation at 50 °C and 100 mbar. Then, the synthesis gel was precrystallized at 90 °C for 20 h under reflux and stirring, and subsequently hydrothermally crystallized at 170 °C for 7 days under autogenous pressure. The zeolitic product was recovered by washing with deionized water and centrifugation (10 min at 6000 rpm) until the pH of the aqueous supernatant was neutral. Then,

the solid sample was dried overnight at 90 ºC and calcined under static air at 550 °C (1.8 °C/min) for 5 h. For the catalysts preparation, the metal precursor (gallium (III) nitrate hydrate ($Ga(NO_3)_3$. xH_2O, Sigma Aldrich, 99.9%) was first dissolved in water and then the supports (n-ZSM-5 and silicalite-1) were added to this solution, using the ratio of 1 g of support per 10 mL of solution. The solution was kept under stirring (200 rpm) at 60 ºC for 6 and then the solvent was removed on a rotary evaporator. The recovered materials were calcined at 550 ºC for 4 h in air (heating rate of 1.8 ºC/min).

2.2. Catalysts characterization

X-ray diffraction (XRD) patterns of the catalysts were recorded on an Empyrean PANalytical diffractometer with Cu (Kα = 1.54 Å) radiation covering 2Θ from 5 ° to 50 ° with a step size of 0.0263º and a net time per step of 957 s, in addition to a voltage of 45 kV and current of 40 mA. Argon physisorption analyses were performed at − 186 °C on a Micromeritics 3Flex instrument, and all samples were degassed under a vacuum at 300 °C for 5 h before the measurements. The specific surface area (S_{BET}) was calculated using BET equation (between 0.05 and 0.16 of relative pressure) and the Non-Local DFT (NL-DFT) model was applied in the adsorption branch to determine the pore size distribution. The total pore volume (V_T) of samples was calculated at a relative pressure (P/P_0) of 0.99 and the micropore volume (V_{MIC}) was determined from the NL-DFT cumulative pore volume versus pore size data. The microporous surface area (S_{MIC}) was determined according to literature procedure [26] and the non-microporous surface area ($S_{MES+EXT}$) was calculated as the difference between the S_{BET} and the S_{MIC}.

Transmission electron microscopy (TEM) was performed on a JEOL JEM 1400 microscope at 120 kV. Field emission scanning electron microscopy (FE-SEM) was performed on a JEOL JSM-7900 F microscope. The mean nanoparticles sizes were determined using ImageJ software by counting around 100 particles in the images of each sample. The surface acidity of the materials was determined by Fourier-transform infrared spectroscopy (FTIR) spectroscopy of adsorbed pyridine in a house-made system. The spectra were recorded with a Jasco-4600 instrument equipped provided with a TGS detector with 128 scans at a resolution of 4 cm^{-1}. Prior to the pyridine adsorption, a self-supported wafer (15 $mgcm^2$) of the materials was activated under vacuum at 525 °C for 1 h. Then, pyridine was adsorbed on the catalysts at 150 °C and the thermal desorption process was performed at 150, 250, 350 and 450 °C with a ramp of 10 °C/min, under high vacuum conditions for 20 min at each temperature. Concentrations of Brønsted (BAS) and Lewis (LAS) acid sites were calculated using the molar extinction coefficients reported by Zholobenko et al. [27] (ξ_{BAS} = 1.09 cm/μmol and ξ_{LAS}= 1.71 cm/μmol for ZSM-5). Thermogravimetry analysis (TGA) in air of the spent catalysts was carried out on a NETZSCH STA 449F3 instrument with heating rate of 10 ºC/min from room temperature to 900 ºC.

2.3. Catalytic performance

Propane dehydrogenation experiments were carried out in a 316 stainless steel fixed-bed reactor (9 mm in diameter, Microactivity-Reference system, PID Eng Tech), under atmospheric pressure. The reaction temperature (550 ºC) was measured by a thermocouple placed above the catalyst bed, and both temperature and pressure were controlled by an automatic process-variable control system. First, the catalyst sample (0.1 g, sieve fraction of 0.28 – 0.5 mm) was placed in the reactor and the system was heated until reaching the reaction temperature, using a flow rate of 50 mL/min of N_2. When the temperature was stabilized, the reactant was introduced into the reactor at a flow rate of 50 mL/min, consisting of 10 vol% propane and 90 vol% of N_2. The gas products were analyzed using an Agilent 490 Micro-Gas chromatograph. The carbon balance was higher than 97% in all the experiments.

The propane conversion (Eq. 1), propylene selectivity (Eq. 2) and yield (Eq. 3) were calculated on carbon basis as follows:

$$Propane\quad conversion\quad (\%) = \frac{moles\quad of(CH_4 + 2\times C_2H_4 + 2\times C_2H_6 + 3\times C_3H_6)}{moles\quad of(CH_4 + 2\times C_2H_4 + 2\times C_2H_6 + 3\times C_3H_6 + 3\times C_3H_8)}\times 100\% \tag{1}$$

$$Propylene\quad selectivity\quad (\%) = \frac{3\times moles\quad of\quad C_3H_6}{moles\quad of(CH_4 + 2\times C_2H_4 + 2\times C_2H_6 + 3\times C_3H_6)}\times 100\% \tag{2}$$

$$Propylene\quad yield\quad (\%) = \frac{3\times moles\quad of\quad C_3H_6}{moles\quad of(CH_4 + 2\times C_2H_4 + 2\times C_2H_6 + 3\times C_3H_6 + 3\times C_3H_8)}\times 100\% \tag{3}$$

The deactivation parameter, estimated from the drop in the propane conversion during the reaction, was calculated according to the following equation (Eq. 4) for a better comparison of the stability of the catalysts.

$$Deactivation\quad parameter\quad (\%) = \frac{Conversion_{initial} - Conversion_{final}}{Conversion_{initial}}\times 100\% \tag{4}$$

3. Results and discussion

3.1. Catalysts properties

Different metal oxide- and Pt-containing n-ZSM-5 catalysts were prepared to evaluate the effect of their textural and acidic properties on the propane dehydrogenation reaction. The catalysts included MgO-n-ZSM-5, CaO-n-ZSM-5, SnO_2-n-ZSM-5, and TiO_2-n-ZSM-5. Additionally, Pt was incorporated over the prepared metal oxide-containing n-ZSM-5 samples. The catalyst comprising Pt on the parent zeolite support was also characterized and tested in the reaction as reference material. In addition, four Ga-containing MFI catalysts, one with Ga incorporated during the hydrothermal synthesis (2.8% Ga-MFI (nSH)), and the other three loaded with Ga by wet impregnation method (7.4% Ga-n-ZSM-5, 2.8% Ga-n-ZSM-5 and 2.8% Ga-Silicalite-1), were prepared to investigate the effect of the location of Ga species and the concentration of acid sites on their catalytic performance.

The XRD patterns of the reference sample Pt-n-ZSM-5, Pt-metal oxides containing n-ZSM-5 and Ga-containing catalysts exhibited the characteristic diffraction peaks corresponding to the typical MFI zeolite topology, according to the IZA database (7.9º, 8.8º, 13.3º, 14.1º, 14.9º, 16.1º, 23.2º, 24.1º, 30.3º), indicating that the crystalline structure was maintained after the metal additions [28]. However, the X-ray diffraction intensities of the impregnated samples slightly decreased, probably due to the coverage effect of the added metallic species. This peak shielding effect can be related with the relatively high metal oxide loading and its preferential location over the outer part of the zeolite crystals. The diffraction peaks of the Ga-MFI (nSH) catalyst show a lower intensity compared to the 2.8% Ga-n-ZSM-5, 7.4% Ga-n-ZSM-5, and 2.8% Ga-silicalite-1 samples due to the smaller crystal domains

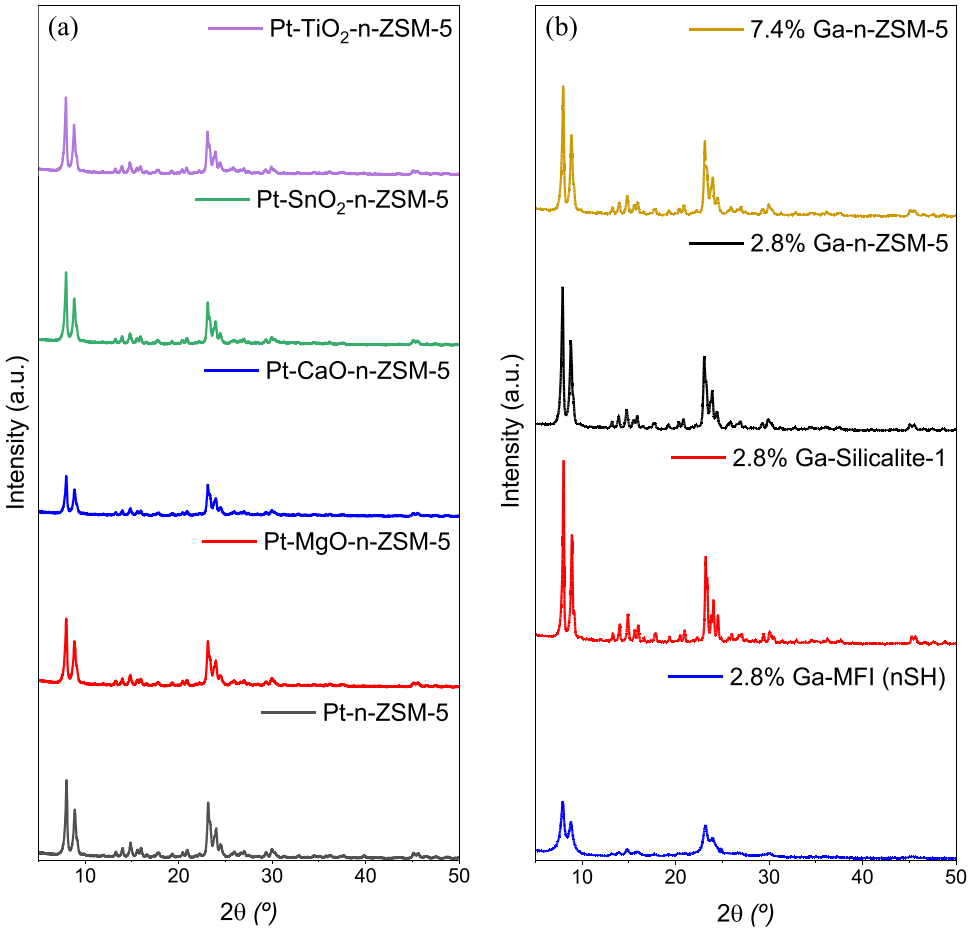

Fig. 1. XRD patterns of the (a) Pt-metal oxides-containing n-ZSM-5 catalysts and (b) Ga-containing MFI catalysts.

Table 1
Textural properties of the catalysts from Ar adsorption/desorption isotherms.

Catalyst	S_{BET} (m^2/g)	S_{MIC} (m^2/g)	$S_{MES+EXT}$ (m^2/g)	V_T (cm^3/g)	V_{MIC} (cm^3/g)
n-ZSM-5	399	282	117	0.52	0.18
Pt-n-ZSM-5	409	276	133	0.57	0.17
Pt-MgO-n-ZSM-5	349	225	124	0.48	0.14
Pt-CaO-n-ZSM-5	302	210	92	0.45	0.13
Pt-SnO_2-n-ZSM-5	379	263	116	0.56	0.16
Pt-TiO_2-n-ZSM-5	373	253	120	0.50	0.16
2.8% Ga-MFI (nSH)	432	238	194	0.55	0.15
2.8% Ga-Silicalite-1	443	273	170	0.39	0.17
2.8% Ga-n-ZSM-5	386	273	113	0.59	0.17
7.4% Ga-n-ZSM-5	402	282	120	0.63	0.18

displayed by the nanosheet morphology. On the other hand, no peaks related to the different metal oxides, neither to Pt or Ga were observed in the catalysts, except for a small peak at 39.8º in the Pt-n-ZSM-5 catalyst corresponding to Pt (111), indicating that the metals were well dispersed on the zeolite surface.

The textural properties of the catalysts determined by Argon (−186 ºC) adsorption-desorption analyses are summarized in Table 1, and the isotherms are shown in Fig. S1. The catalysts derived from the n-ZSM-5 and Silicalite-1 samples exhibit the typical I(b) isotherms [29] characteristic of microporous materials with high adsorption at low relative pressures. Moreover, all these samples exhibit significant adsorption at relative pressures higher than 0.85, which is associated with intercrystalline adsorption [29]. On the contrary, the sample 2.8% Ga-MFI (nSH) displays a type IV isotherm, with a significant adsorption at intermediate relative pressures (P/P_0 = 0.4–0.8), suggesting the presence of mesopores due to its morphological characteristics (nanosheets). Regarding the textural properties, in general, the incorporation of metal oxide over the zeolitic nanocrystals generated a decrease in both S_{BET} and V_T and V_{MIC} respecting the parent Pt-n-ZSM-5, due to the partial blockage of the pores by the metal oxide nanoparticles. The decrease in micropore volume was less accentuated in the case of SnO_2 and TiO_2, indicating that these oxides could be preferentially located on the external surface of the zeolite. On the contrary, the most remarkable changes were observed after the incorporation of CaO and MgO, which could indicate the preferential location of the CaO and MgO on the zeolitic micropores. Finally, regarding the Ga-containing catalysts, the 2.8% Ga-MFI (nSH) catalyst exhibited a high S_{BET} and $S_{MES+EXT}$ due to its unique nanosheet morphology, Ga-silicalite-1 showed similar textural properties to previous works [19] and in the case of Ga_2O_3 loading, the V_T was higher compared to the parent n-ZSM-5, while the S_{BET}, $S_{MES+EXT}$ and V_{MIC} remained almost unchanged. This could be due to the formation of intergranular mesopores during the accumulation of nanocrystal particles [30] in the case of Ga-n-ZSM-5 samples.

FTIR spectroscopy using pyridine as a probe molecule was used to estimate the acidic properties of the catalysts. Fig. S2 shows the pyridine vibration region FTIR spectra recorded after pyridine desorption at 150 ºC. The concentrations of Brønsted (C_{BAS}), Lewis (C_{LAS}), total acid (C_T) sites, and the C_{BAS}/C_{LAS} ratio are summarized in Table 2. All Pt-oxide-containing zeolite catalysts showed a lower concentration of BAS than the parent Pt-n-ZSM-5, especially the catalyst containing MgO and CaO. On the other hand, the concentration of LAS increased after metal-oxide

Table 2
Acidic properties of the catalysts.

Catalyst	C_{BAS}[a] (mmol/g)	C_{LAS}[a] (mmol/g)	C_{BAS}/C_{LAS}	C_T (mmol/g)	Fraction of strong BAS[b] (%)	Fraction of strong LAS[b] (%)
Pt-n-ZSM-5	0.212	0.076	2.77	0.288	69	39
Pt-MgO-n-ZSM-5	0.068	0.325	0.21	0.393	46	37
Pt-CaO-n-ZSM-5	0.033	0.209	0.16	0.242	19	29
Pt-SnO_2-n-ZSM-5	0.131	0.131	1.00	0.262	55	19
Pt-TiO_2-n-ZSM-5	0.177	0.107	1.666	0.283	64	31
2.8% Ga-MFI (nSH)	0.130	0.187	0.69	0.317	72	57
2.8% Ga-Silicalite-1	0.000	0.100	0.00	0.100	-	3
2.8% Ga-n-ZSM-5	0.181	0.112	1.62	0.292	65	38
7.4% Ga-n-ZSM-5	0.180	0.096	1.88	0.276	61	43

[a] C_{BAS} and C_{LAS} measured at 150 °C.
[b] Acid site concentration at 350 ℃ in relation to that at 150 ℃.

loading, particularly in the samples Pt-MgO-n-ZSM-5 and Pt-CaO-n-ZSM-5 samples, while it slightly decreased in the case of SnO_2 addition. Further insights regarding the Lewis acid sites modification after oxide loading can be inferred analyzing the band shift of the parent zeolite at (1621 cm^{-1}), which is attributed to pyridine interaction with the Lewis acid sites. This band is practically absent in the case of samples impregnated with MgO and CaO, while a new band in the region at 1610 cm^{-1} appears, to a greater or lesser extent, after the incorporation of all metals (Fig. S2a). The shift of the 1621 cm^{-1} band position towards lower wavelengths is related to the appearance of weaker Lewis centers, so it can be stated that the incorporation of metal oxides provides the Pt-n-ZSM-5 sample with weaker Lewis acidity. Therefore, this Lewis acid strength increases following this trend: Pt-CaO-n-ZSM-5 < Pt-TiO_2-n-ZSM-5 < Pt-MgO-n-ZSM-5 < Pt-SnO_2-n-ZSM-5 < Pt-n-ZSM-5.

Among the Ga-containing catalysts, the 7.4% and 2.8% Ga-n-ZSM-5 samples showed the highest concentration of BAS (around 0.180 mmol/g). Regarding the LAS, the peaks corresponding to pyridine coordinated to Lewis's acid sites (PyL at 1621 and 1456 cm^{-1}) are even larger than in the parent Pt-n-ZSM-5, confirming the higher concentration of these Lewis acid sites. Moreover Ga-MFI (nSH) presented the highest concentration of LAS (0.187 mmol/g), as a consequence of the abundant framework-Ga species, which is consistent with previous works [31,32]. On the other hand, as expected, no BAS was detected in Ga-Silicalite-1 catalyst (Fig. S2b). Compared to the parent Pt-n-ZSM-5, the decrease in the amount of the BAS observed in the 2.8% and 7.4% Ga-n-ZSM-5 catalysts was attributed to blockage of the channels and pore mouths by Ga_2O_3 and other extra-crystalline species [23], whereas the increase in LAS is explained by the conversion of BAS related to the zeolite framework into LAS, associated with the incorporated Ga species [33]. The differences in Ga species in these materials resulted in the C_{BAS}/C_{LAS} ratio being more than twice larger in the 2.8% and 7.4% Ga-n-ZSM-5 catalysts than in Ga-MFI (nSH), despite the fact that both materials had a similar concentration of total acid sites (around 0.3 mmol/g).

The concentration of BAS and LAS at desorption temperatures of 150, 250, 350 and 450 ℃ are shown in Fig. S3. The fraction of strong BAS and LAS was also estimated as a function of the acid concentration of the retained pyridine after desorption at 150 °C and 350 °C (Table 2). As previously suggested, the concentration of strong BAS was higher in the Pt-n-ZSM-5 (69%) than in the samples where the oxides were incorporated (19–64%). The fraction of strong LAS also decreased from 39% to 19–37% after the metal-oxide addition in Pt-n-ZSM-5. On the other hand, Ga-MFI (nSH) showed a higher fraction of LAS than 2.8% and 7.4% Ga-n-ZSM-5 samples due to the higher abundance of framework Ga species [31], while Ga-Silicalite-1 material mainly showed the weakest concentration and fraction of acid sites. This LAS weakening for the Ga-Silicalite-1 sample can be also seen in the PyL band displacement from 1456 cm^{-1} to 1447 cm^{-1}, and in the appearance of a PyL band at 1589 cm^{-1} (Fig. S2).

Fig. 2 shows the SEM images of the Pt-containing catalysts and the mean nanoparticle size distribution. The Pt-n-ZSM-5 catalyst had the largest mean nanoparticle size (19.6 ± 10.3 nm), while the catalysts prepared using the metal oxides-n-ZSM-5 had smaller mean nanoparticle size with narrower size distribution. Among the catalysts prepared from metal oxides-n-ZSM-5, Pt-MgO-n-ZSM-5 and Pt-CaO-n-ZSM-5 had the smallest mean nanoparticle size, between 7.3 and 7.9 ± 2.2–2.5 nm, indicating the possible occurrence of ion-exchange with protons of the parent zeolite, as reported in literature [34]. Additionally, the small average nanoparticle size obtained with the Pt catalyst prepared using SnO_2 and TiO_2-n-ZSM-5 could be attributed to the lower acidity (mainly BAS) of these materials, since it has been reported that weakly acidic supports can improve the dispersion of Pt due to an increased metal-support interaction [35]. In addition, it is important to highlight that the in catalysts prepared with SnO_2, and TiO_2, the nanoparticles observed in the images could correspond to both metals (Pt and the reduced metal from the oxide) and/or by the bimetallic alloys between them, since these oxides could have been partially or completely reduced during the H_2 reduction method [36–39].

As shown in Fig. 3, TEM images of the oxides-containing n-ZSM-5 catalysts also confirm that the crystal size (20–50 nm) of the Pt-n-ZSM-5 was not altered by the metal oxide loading, and that the oxides were well dispersed in the zeolite, as no large particle agglomerations were observed on the catalysts (Fig. 3a-d). Energy dispersive X-ray spectrometry (EDS) elemental mapping images (Fig. S4) also shows the high and homogeneous dispersion of the metal oxides in n-ZSM-5 zeolite. Although no significant variation was observed in the textural properties of the parent Pt-n-ZSM-5 sample after impregnation with SnO_2 and TiO_2 (Table 1), small nanoparticles with sizes ranging from 5 to 10 nm were detected in the TEM micrographs. Additionally, the TEM images of the Pt-oxide-containing catalysts (Fig. 3e-i) show the high dispersion and the small sizes of the nanoparticles, while areas with a high concentration of nanoparticles were also detected in the Pt-CaO-n-ZSM-5 catalyst, as can be seen in Fig. 3g. A high Ga dispersion was also observed in the catalysts (Fig. S4).

3.2. Catalytic performance

Propane dehydrogenation was first carried out at 550 ℃ for 4 h over the Pt-oxides- catalysts. The catalytic performance results during the reaction time of the parent Pt-n-ZSM-5 and the Pt-oxides-n-ZSM-5 catalysts are shown in Fig. 4. In the literature [40,41], it was reported that the LAS are the active sites for the dehydrogenation reaction, while both catalytic cracking and coke formation could be catalyzed through BAS and LAS.

A time-averaged (4 h) propane conversion of 16% and propylene selectivity of 83% was obtained with Pt-n-ZSM-5 catalyst (Fig. 4), resulting in a propylene yield of 13%. However, the high concentration of BAS favored the formation of a large amount of carbonaceous deposits on the catalyst surface, resulting in a loss of catalytic activity during the reaction time, as will be discussed below and supported by the large error bar of the results. The catalytic activity did not improve with the Pt catalysts prepared from the oxide-containing n-ZSM-5 and only the Pt-CaO-n-ZSM-5 catalyst achieved conversions close to 10%, although

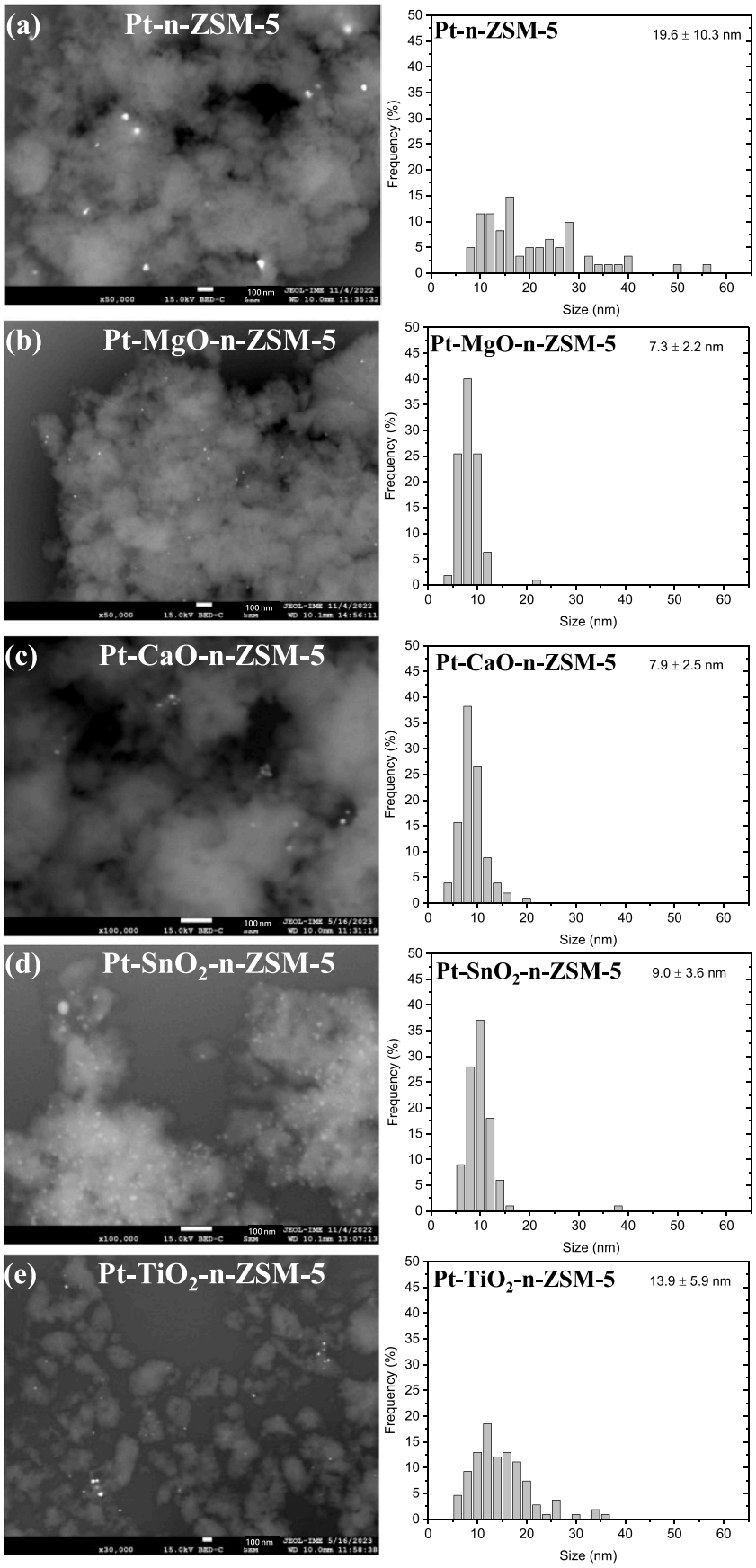

Fig. 2. SEM images and histograms of metal particle size distribution of the Pt-containing catalysts.

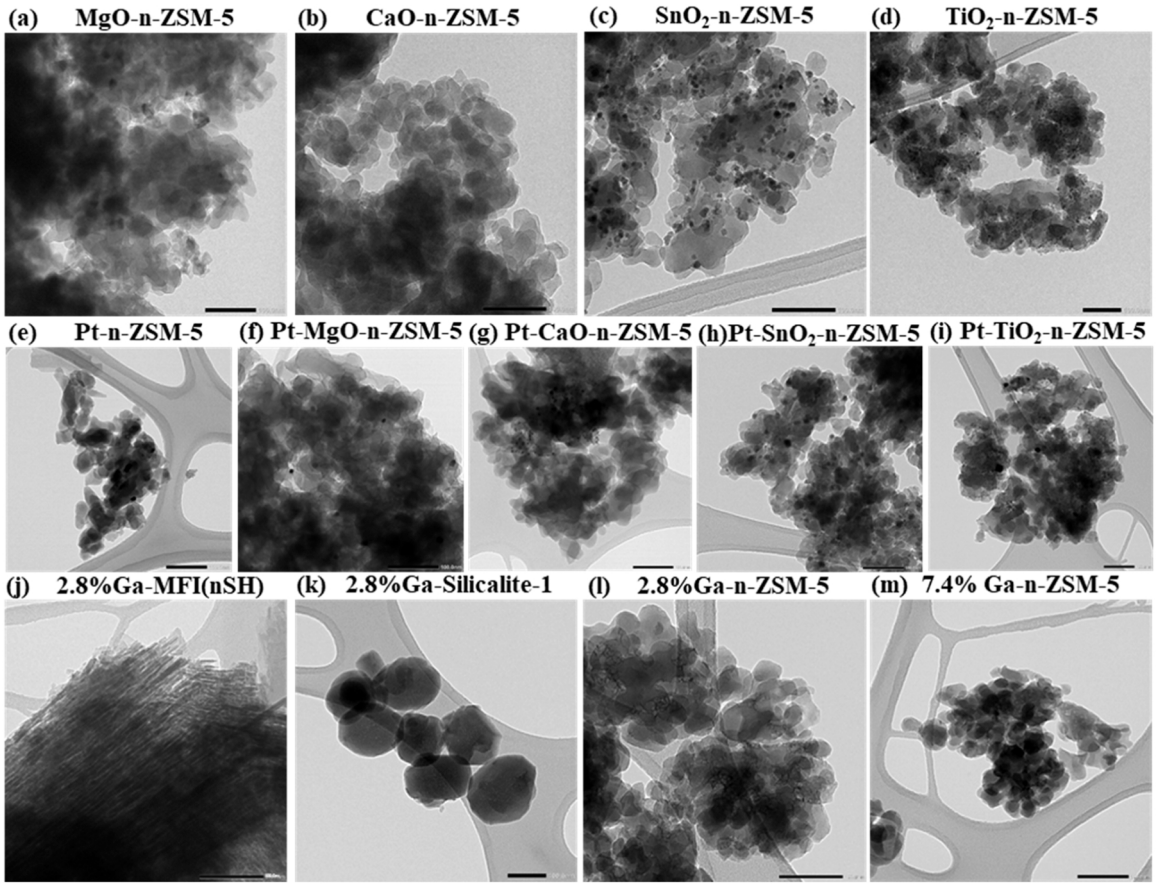

Fig. 3. TEM images of (a-d) oxides-containing catalysts, (e-i) Pt-containing catalysts and (j-m) Ga-containing catalysts.

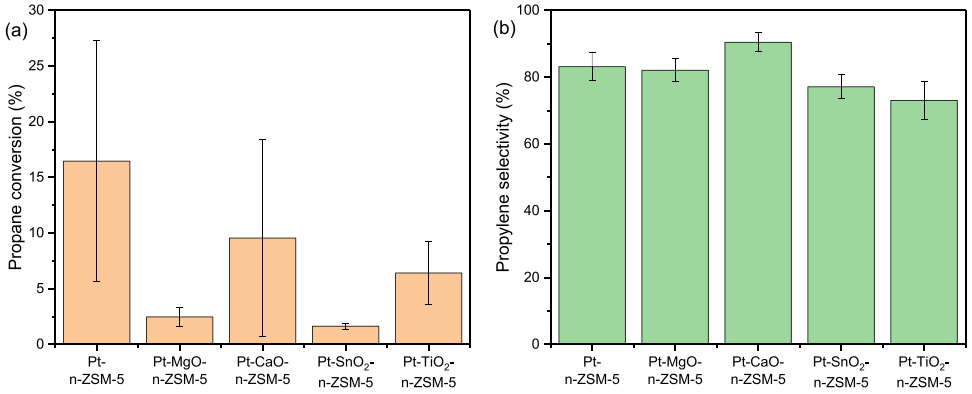

Fig. 4. (a) Propane conversion and (b) propylene selectivity of the parent Pt-n-ZSM-5 and Pt-oxides-n-ZSM-5 catalysts.

the loss of activity was remarkable (high error bar), as discussed later.

Fig. 5 shows the time-averaged (4 h) catalytic performance of the Ga-containing catalysts. The Ga-MFI (nSH) catalyst showed the highest catalytic performance in propane dehydrogenation, achieving around 9% conversion and 80% propylene selectivity. These results could be attributed to the synergistic interaction between the BAS and LAS sites [42] and a higher Lewis acid strength (Table 2), which is associated with a higher activity in the dehydrogenation of light paraffins [23,43]. The catalytic activity of the 2.8% and 7.4% Ga-n-ZSM-5 materials was lower than that of Ga-MFI (nSH), 6% and 8% of propane conversion and 71% and 63% of propylene selectivity, respectively, probably due to its higher BAS concentration and lower LAS, with a C_{BAS}/C_{LAS} site ratio of 1.62 and 1.88, respectively, much higher than of the Ga-MFI (nSH) catalyst (0.69). Finally, the Ga-Silicalite-1 catalyst showed an intermediate activity between the two previous Ga catalysts (7% of conversion and 75% of propylene selectivity), demonstrating that the Lewis acidity of this zeolitic support is key to achieving a higher conversion and selectivity than the Al^{3+} MFI zeolitic structure. Thus, blank experiments performed with the latter (data not shown) led to 2% conversion and 32% of propylene selectivity. Consequently, the propylene yield had the following sequence: Ga-MFI (nSH) $>$ 2.8% Ga-Silicalite-1 $>$ 2.8% and 7.4% Ga-n-ZSM-5. The results suggest that the presence of lower concentrations of BAS coupled with the presence of strong LAS leads to higher propane conversion and propylene selectivity, indicating that the incorporation of Ga framework species into the zeolite is crucial to improve the catalytic performance. The hypothesis that there may be a bifunctional mechanism between BAS and LAS that favours the catalytic performance in the propane dehydrogenation

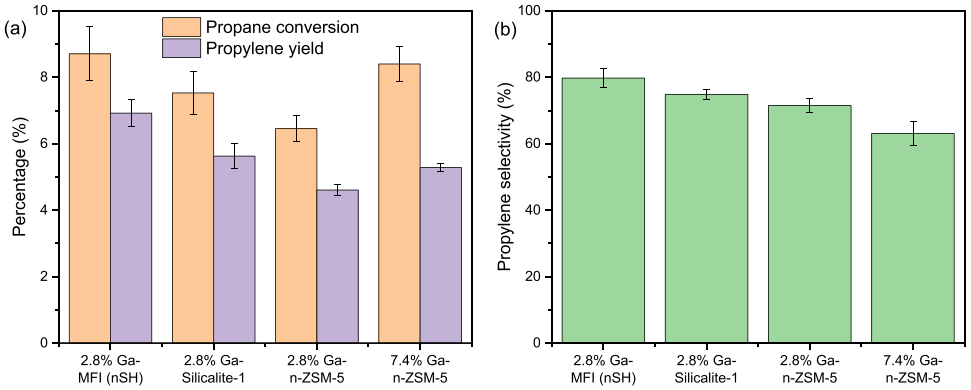

Fig. 5. (a) Propane conversion and propylene yield and (b) propylene selectivity of Ga-containing catalysts.

reaction, suggested by Choi et al. [21] would also support our results. Previous studies have reported similar results to those obtained in this work for various gallosilicate MFI catalysts with different acidities [43]. Propane conversion was maintained in a range of 9–13% and the propylene selectivity varied between 60% and 90%.

3.3. Catalysts stability

The catalysts that presented the best results in the previous section were selected for a more detailed analysis of their stability. The results of the parent Pt-n-ZSM-5 zeolite were also included for comparison. The propane conversion and the propylene selectivity and yield for the selected catalysts with the time on stream (TOS) are shown in Fig. 6. The initial propane conversion of Pt-n-ZSM-5 was around 35% with a propylene selectivity of 76. %. However, this catalyst showed an evident loss of activity during the first hours of reaction and the propane conversion decreased from 35% to 6% after 4 h time on stream, resulting in a decrease in propylene yield from 27% to 5%. Pt-CaO-n-ZSM-5 also showed a loss of catalytic activity during the first hours of the reaction, with an initial conversion of 27% and a decrease in conversion to 2% after 4 h time on stream. Interestingly, the highest propylene selectivity was achieved with this catalyst, possibly due to its lowest BAS concentration, and that was barely reduced during the reaction, but due to the loss of activity, the propylene yield decreased from 23% to 2%. In contrast, the 2.8% and 7.4% Ga-n-ZSM-5 samples, Ga-MFI (nSH), and 2.8% Ga-Silicalite-1 catalysts did not exhibit any remarkable loss of activity stability in the propane dehydrogenation reaction after 4 h time on stream, clearly demonstrating the superior stability of these catalysts compared to the others.

To compare the catalytic performance of all the materials tested in this work, Fig. 7a shows the selectivity-conversion results. The best catalysts are shown in the inner box with dotted lines. Additionally, Fig. 7b shows the stability values of the catalysts in terms of the deactivation parameter or coefficient measured by Eq. 4. The cross-measurement of both parameters indicates the overall productivity of the catalysts used. Although some of the catalysts, such as Pt-n-ZSM-5,

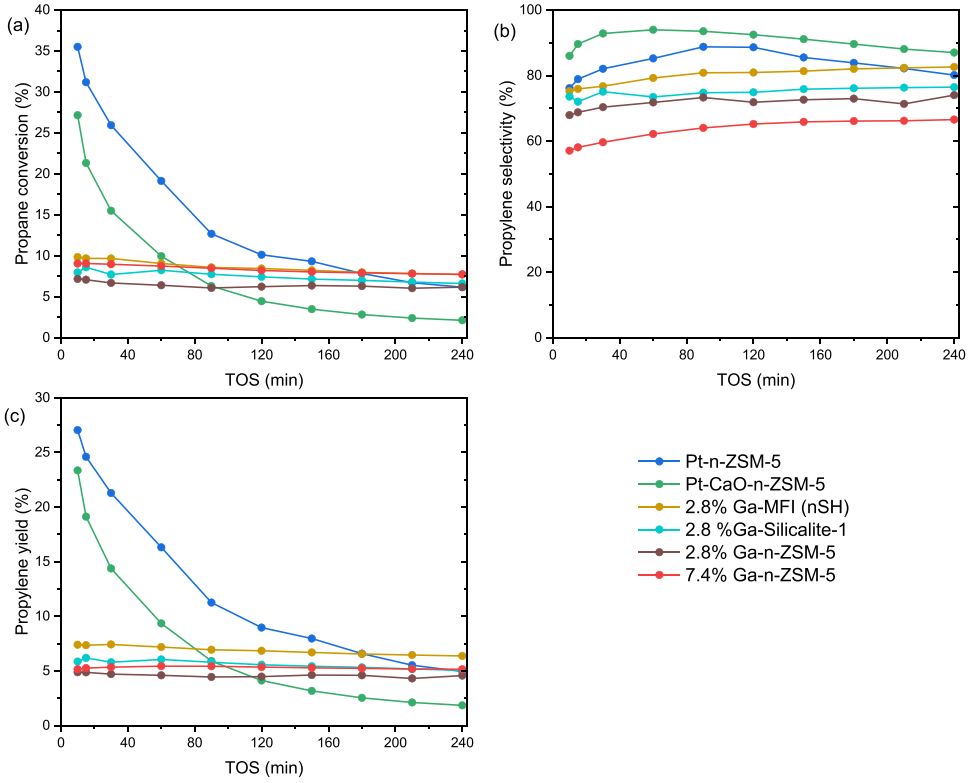

Fig. 6. Comparison of (a) propane conversion, (b) propylene selectivity and (c) propylene yield of different catalysts with time on stream (TOS).

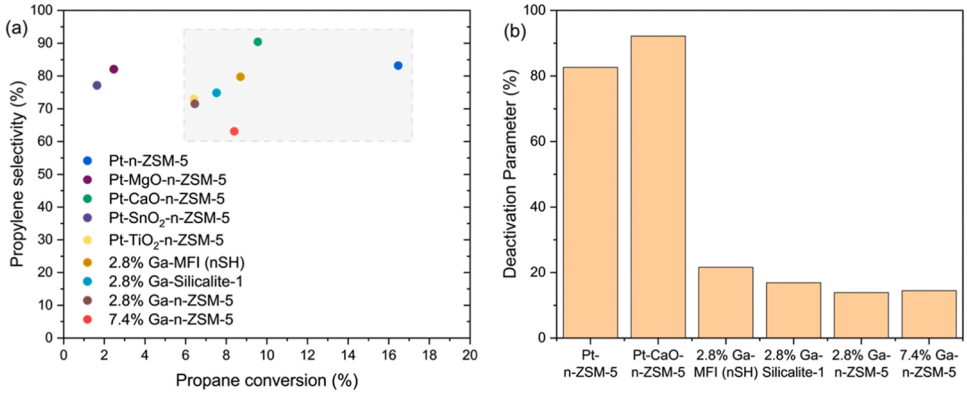

Fig. 7. (a) Selectivity-conversion results and (b) deactivation parameter of different catalysts.

could be interesting from the point of view of catalytic activity, the high value of the deactivation coefficient discourages their use. A similar result is obtained for the Pt-CaO-n-ZSM-5 catalyst. On the contrary, Ga-containing catalysts exhibit a good balance between catalytic activity (propane conversion and selectivity towards propylene) and deactivation inhibition, thus showing an overall superior catalytic performance. Furthermore, all the Ga-containing catalysts (2.8% and 7.4% Ga-n-ZSM-5, 2.8% Ga-MFI (nSH), and 2.8% Ga-Silicalite-1) reached lower deactivation values (14–22%) than those observed with Pt catalysts, thus highlighting their superior stability in the propane dehydrogenation reaction. The explanation may be, as mentioned above, the synergy between the Brønsted and Lewis centers and also in a higher stability of the catalysts due to the overall lower acidity of the zeolitic supports in which Al^{3+} is substituted by Ga^{3+} [44].

TGA was employed to determine the coke deposition over the spent catalysts after 4 h time on stream at 550 ºC. The change of weight percent as a function of temperature is shown in Fig. 8. The first weight loss at temperatures below 200 ºC is attributed to adsorbed water, while the others are due to coke decomposition. From these profiles, it can be observed that the amount of coke deposition follows the order 2.8% Ga-n-ZSM-5 (4.57%) < 7.4% Ga-n-ZSM-5 (4.79%) < Pt-CaO-n-ZSM-5 (5.87%) < 2.8% Ga-Silicalite-1 (6.16%) < 2.8% Ga-MFI (nSH) (6.94%) < Pt-n-ZSM-5 (7.14%). As the amount of coke is affected by the propane conversion, the Pt-n-ZSM-5 catalyst showed the highest amount of coke, possibly due to the higher concentration of total acid sites and mainly due to its strong Brønsted acid sites.

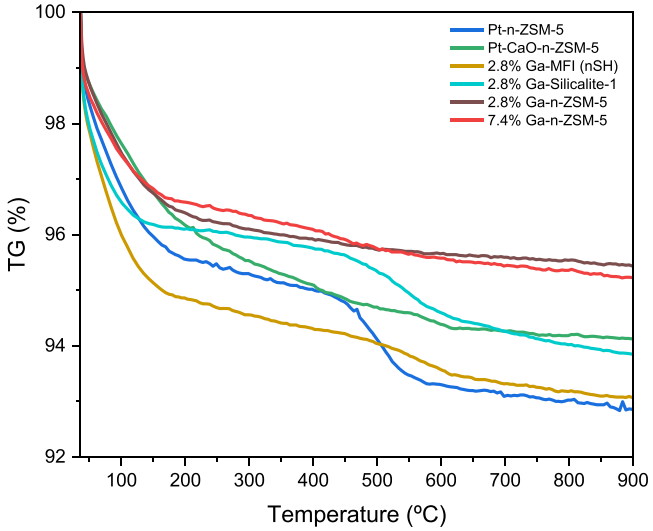

Fig. 8. TGA profiles of the spent catalysts after 4 h time on stream.

4. Conclusions

A series of oxides-n-ZSM-5 catalysts (MgO, CaO, SnO_2, TiO_2) were prepared by wet impregnation method and tested in propane dehydrogenation (PDH) reaction to produce propylene. Pt was also loaded on these catalysts and tested in propane dehydrogenation (PDH) reaction to produce propylene. On the other hand, Ga-containing catalysts were prepared by hydrothermal synthesis (Ga-MFI (nSH)) and by wet impregnation method (2.8% Ga-Silicalite-1, 2.8%Ga-n-ZSM-5, and 7.4% Ga-n-ZSM-5) and the catalytic performance of these materials was also evaluated in PDH. Characterization with XRD, Ar physisorption, TEM, SEMand FTIR of adsorbed pyridine techniques reveal that the oxide addition did not change the morphology of the parent Pt-n-ZSM-5 and that the oxides were well dispersed on the zeolite. The oxides addition decreased the concentration of BAS while remarkably increasing the strength of the LAS. Pt catalyst prepared using metal oxides-n-ZSM-5 showed a smaller mean nanoparticle size than reference Pt-n-ZSM-5, which was attributed to the lower acidity (mainly BAS) of these materials that favored the dispersion of Pt nanoparticles. The characterization of the Ga-containing catalysts also revealed a high metal dispersion and confirmed the morphology of the prepared materials. In addition, Ga-MFI (nSH) presented a higher fraction of LAS than 2.8% Ga-n-ZSM-5, 7.4% Ga-n-ZSM-5 and 2.8% Ga-Silicalite-1 due to the higher abundance of framework Ga species.

Pt-containing catalysts achieved high conversions at the start of the reaction, but these materials were rapidly deactivated by coke formation. Ga-containing MFI catalysts showed a superior stability in the PDH reaction. Among them, Ga-MFI (nSH) catalysts achieved the highest catalytic performance in PDH (9% conversion and 80% propylene selectivity), due to the synergy between the BAS and LAS and the higher fraction of strong LAS. The results denote the great potential of Ga MFI zeolites as catalysts in PDH reactions and highlight the need to tune the textural and acidity properties of the catalysts to improve catalytic performance.

CRediT authorship contribution statement

Adriana S. Oliveira: Methodology, Investigation, Writing – original draft preparation. **Jennifer Cueto:** Methodology, Investigation, Validation, Writing – review & editing. **María del Mar Alonso-Doncel:** Methodology, Validation, Writing – review & editing. **Martin Kubů:** Validation, Writing – review & editing. **Jiří Čejka:** Validation, Writing – review & editing. **David. P. Serrano:** Conceptualization, Methodology, Validation, Writing – review & editing, Supervision, Funding. **Rafael A. García-Muñoz:** Conceptualization, Methodology, Validation, Writing – original draft preparation, Writing – review & editing, Supervision. All authors read and approved the final manuscript and agreed with its contents and publication in the final form.

Declaration of Competing Interest

The authors declare that they have no known competing financial interests or personal relationships that could have appeared to influence the work reported in this paper.

Data availability

Data will be made available on request.

Acknowledgement

Authors gratefully acknowledge European Research Council Horizon 2020 research an innovation program TODENZE project (ERC-101021502). Adriana S. Oliveira thanks the Ministry of Universities; The Recovery, Transformation and Resilience Plan, and the Autonomous University of Madrid for a research grant (CA1/RSUE/2021–00836). MK and JC thank the Czech Science Foundation for funding this research through the ExPro project (19–27551X) and OP VVV "Excellent Research Teams", project no. Z.02.1.01/0.0/0.0/15_003/0000417 – CUCAM from Ministerstvo Školství, Mládeže a Tělovýchovy. The work was also supported by ERDF/ESF project TECHSCALE (No. CZ.02.01.01/00/22_008/0004587) and Investigo Program (Nº Exp 09-PIN1-00006.5/2022) funded by European Union - Next Generation EU.

Appendix A. Supporting information

Supplementary data associated with this article can be found in the online version at doi:10.1016/j.cattod.2023.114437.

References

[1] Y. Yuan, C. Brady, L. Annamalai, R.F. Lobo, B. Xu, Ga speciation in Ga/H-ZSM-5 by in-situ transmission FTIR spectroscopy, J. Catal. 393 (2021) 60–69, https://doi.org/10.1016/j.jcat.2020.11.004.
[2] H.M. Torres Galvis, K.P. De Jong, Catalysts for production of lower olefins from synthesis gas: a review, ACS Catal. 3 (2013) 2130–2149, https://doi.org/10.1021/cs4003436.
[3] A. Akah, M. Al-Ghrami, Maximizing propylene production via FCC technology, Appl. Petrochem. Res. 5 (2015) 377–392, https://doi.org/10.1007/s13203-015-0104-3.
[4] Y. Dai, X. Gao, Q. Wang, X. Wan, C. Zhou, Y. Yang, Recent progress in heterogeneous metal and metal oxide catalysts for direct dehydrogenation of ethane and propane, Chem. Soc. Rev. 50 (2021) 5590–5630, https://doi.org/10.1039/d0cs01260b.
[5] R. Rabenhorst, On Purpose, What's driving new propane dehydrogenation projects in North America? Nexant (2019).
[6] J.J.H.B. Sattler, J. Ruiz-Martinez, E. Santillan-Jimenez, B.M. Weckhuysen, Catalytic dehydrogenation of light alkanes on metals and metal oxides, Chem. Rev. 114 (2014) 10613–10653, https://doi.org/10.1021/cr5002436.
[7] L. Ni, R. Khare, R. Bermejo-Deval, R. Zhao, L. Tao, Y. Liu, J.A. Lercher, Highly active and selective sites for propane dehydrogenation in zeolite Ga-BEA, J. Am. Chem. Soc. 144 (2022) 12347–12356, https://doi.org/10.1021/jacs.2c03810.
[8] Y. Wang, Z.P. Hu, X. Lv, L. Chen, Z.Y. Yuan, Ultrasmall PtZn bimetallic nanoclusters encapsulated in silicalite-1 zeolite with superior performance for propane dehydrogenation, J. Catal. 385 (2020) 61–69, https://doi.org/10.1016/j.jcat.2020.02.019.
[9] M. Sajad, Y. Zhang, M. Kubů, M. Mazur, R. Bulanek, J. Čejka, Direct dehydrogenation of propane over Pd nanoparticles encapsulated within IPC zeolites with tunable pore sizes, Appl. Mater. Today 29 (2022), 101644, https://doi.org/10.1016/j.apmt.2022.101644.
[10] A.H. Motagamwala, R. Almallahi, J. Wortman, V.O. Igenegbai, S. Linic, Stable and selective catalysts for propane dehydrogenation operating at thermodynamic limit, Sci. (80-.) 373 (2021) 217–222, https://doi.org/10.1126/science.abg7894.
[11] S. Goel, Z. Wu, S.I. Zones, E. Iglesia, Synthesis and catalytic properties of metal clusters encapsulated within small-pore (SOD, GIS, ANA) zeolites, J. Am. Chem. Soc. 134 (2012) 17688–17695, https://doi.org/10.1021/ja307370z.
[12] Y. Zhang, A. Li, M. Sajad, K. Fulajtárová, M. Mazur, M. Kubů, M. Shamzhy, M. Hronec, R. Bulánek, J. Čejka, Imidazolium-type ionic liquid-assisted formation of the MFI zeolite loaded with metal nanoparticles for hydrogenation reactions, Chem. Eng. J. 412 (2021), https://doi.org/10.1016/j.cej.2021.128599.
[13] L. Liu, U. Díaz, R. Arenal, G. Agostini, P. Concepción, A. Corma, Generation of subnanometric platinum with high stability during transformation of a 2D zeolite into 3D, Nat. Mater. 16 (2017) 132–138, https://doi.org/10.1038/nmat4757.
[14] Y. Zhang, M. Kubů, M. Mazur, J. Čejka, Encapsulation of Pt nanoparticles into IPC-2 and IPC-4 zeolites using the ADOR approach, Microporous Mesoporous Mater. 279 (2019) 364–370, https://doi.org/10.1016/j.micromeso.2019.01.018.
[15] L. Liu, M. Lopez-Haro, C.W. Lopes, C. Li, P. Concepcion, L. Simonelli, J.J. Calvino, A. Corma, Regioselective generation and reactivity control of subnanometric platinum clusters in zeolites for high-temperature catalysis, Nat. Mater. 18 (2019) 866–873, https://doi.org/10.1038/s41563-019-0412-6.
[16] P. Hu, W.Z. Lang, X. Yan, X.F. Chen, Y.J. Guo, Vanadium-doped porous silica materials with high catalytic activity and stability for propane dehydrogenation reaction, Appl. Catal. A Gen. 553 (2018) 65–73, https://doi.org/10.1016/j.apcata.2018.01.014.
[17] Y. Gu, H. Liu, M. Yang, Z. Ma, L. Zhao, W. Xing, P. Wu, X. Liu, S. Mintova, P. Bai, Z. Yan, Highly stable phosphine modified VOx/Al2O3 catalyst in propane dehydrogenation, Appl. Catal. B Environ. 274 (2020), https://doi.org/10.1016/j.apcatb.2020.119089.
[18] C.R. Bayense, A.J.H.P. van der Pol, J.H.C. van Hooff, Aromatization of propane over MFI-gallosilicates, Appl. Catal. 72 (1991) 81–98, https://doi.org/10.1016/0166-9834(91)85030-Y.
[19] Y. Wang, Y. Suo, X. Lv, Z. Wang, Z.Y. Yuan, Enhanced performances of bimetallic Ga-Pt nanoclusters confined within silicalite-1 zeolite in propane dehydrogenation, J. Colloid Interface Sci. 593 (2021) 304–314, https://doi.org/10.1016/j.jcis.2021.02.129.
[20] K.M. Dooley, T.F. Guidry, G.L. Price, Control of intrazeolitic gallium cation content and its effects on C2 dehydrogenation in Ga-MFI catalysts, J. Catal. 157 (1995) 66–75, https://doi.org/10.1006/jcat.1995.1268.
[21] V.R. Choudhary, C. Sivadinarayana, A.K. Kinage, P. Devadas, M. Guisnet, H-Gallosilicate (MFI) propane aromatization catalyst influence of calcination temperature on acidity, activity and deactivation due to coking, Appl. Catal. A Gen. 136 (1996) 125–142, https://doi.org/10.1016/0926-860X(95)00277-4.
[22] A. Getsoian, U. Das, J. Camacho-Bunquin, G. Zhang, J.R. Gallagher, B. Hu, S. Cheah, J.A. Schaidle, D.A. Ruddy, J.E. Hensley, T.R. Krause, L.A. Curtiss, J. T. Miller, A.S. Hock, Organometallic model complexes elucidate the active gallium species in alkane dehydrogenation catalysts based on ligand effects in Ga K-edge XANES, Catal. Sci. Technol. 6 (2016) 6339–6353, https://doi.org/10.1039/c6cy00698a.
[23] Y. Fang, X. Su, X. Bai, W. Wu, G. Wang, L. Xiao, A. Yu, Aromatization over nanosized Ga-containing ZSM-5 zeolites prepared by different methods: effect of acidity of active Ga species on the catalytic performance, J. Energy Chem. 26 (2017) 768–775, https://doi.org/10.1016/j.jechem.2017.03.014.
[24] W.G. Kim, J. So, S.W. Choi, Y. Liu, R.S. Dixit, C. Sievers, D.S. Sholl, S. Nair, C. W. Jones, Hierarchical Ga-MFI Catalysts for Propane Dehydrogenation, Chem. Mater. 29 (2017) 7213–7222, https://doi.org/10.1021/acs.chemmater.7b01566.
[25] M. Choi, K. Na, J. Kim, Y. Sakamoto, O. Terasaki, R. Ryoo, Stable single-unit-cell nanosheets of zeolite MFI as active and long-lived catalysts, Nature 461 (2009) 246–249, https://doi.org/10.1038/nature08288.
[26] D.P. Serrano, J. Aguado, Á. Peral, Controlling the generation of hierarchical porosity in ZSM-5 by changing the silanization degree of protozeolitic units, Stud. Surf. Sci. Catal. 174 (2008) 123–128, https://doi.org/10.1016/S0167-2991(08)80162-0.
[27] V. Zholobenko, C. Freitas, M. Jendrlin, P. Bazin, A. Travert, F. Thibault-Starzyk, Probing the acid sites of zeolites with pyridine: quantitative AGIR measurements of the molar absorption coefficients, J. Catal. 385 (2020) 52–60, https://doi.org/10.1016/j.jcat.2020.03.003.
[28] IZA (International Zeolite Association), Database of Zeolite Structures, (n.d.).
[29] M. Thommes, K. Kaneko, A.V. Neimark, J.P. Olivier, F. Rodriguez-Reinoso, J. Rouquerol, K.S.W. Sing, Physisorption of gases, with special reference to the evaluation of surface area and pore size distribution (IUPAC Technical Report), Pure Appl. Chem. 87 (2015) 1051–1069, https://doi.org/10.1515/pac-2014-1117.
[30] M. Al-Eid, L. Ding, D. Sewdan, E. AL-Shafei, R. Al-Ghamdi, A. Alqarawi, E. Alnaimi, Effect of ZSM-5 particle size and framework silica-to-alumina ratio on hexane aromatization, Catal. Res. 2 (2022) 1–19, https://doi.org/10.21926/cr.2204035.
[31] M. Xin, E. Xing, X. Gao, Y. Wang, Y. Ouyang, G. Xu, Y. Luo, X. Shu, Ga substitution during modification of ZSM-5 and its influences on catalytic aromatization performance, Ind. Eng. Chem. Res. 58 (2019) 6970–6981, https://doi.org/10.1021/acs.iecr.9b00295.
[32] S. Altwasser, A. Raichle, Y. Traa, J. Weitkamp, Preparation of gallium-containing catalysts by solid-state reaction of acidic zeolites with elemental gallium, Chem. Eng. Technol. 27 (2004) 1262–1265, https://doi.org/10.1002/ceat.200407044.
[33] V. De, O. Rodrigues, J.G. Eon, A.C. Faro, Correlations between dispersion, acidity, reducibility, and propane aromatization activity of gallium species supported on HZSM5 zeolites, J. Phys. Chem. C. 114 (2010) 4557–4567, https://doi.org/10.1021/jp910642p.
[34] J. Fermoso, H. Hernando, P. Jana, I. Moreno, J. Přech, C. Ochoa-Hernández, P. Pizarro, J.M. Coronado, J. Čejka, D.P. Serrano, Lamellar and pillared ZSM-5 zeolites modified with MgO and ZnO for catalytic fast-pyrolysis of eucalyptus woodchips, Catal. Today 277 (2016) 171–181, https://doi.org/10.1016/j.cattod.2015.12.009.
[35] W. Wannapakdee, T. Yutthalekha, P. Dugkhuntod, K. Rodponthukwaji, A. Thivasasith, S. Nokbin, T. Witoon, S. Pengpanich, C. Wattanakit, Dehydrogenation of propane to propylene using promoter-free hierarchical Pt/silicalite-1 nanosheets, Catalysts 9 (2019), https://doi.org/10.3390/catal9020174.
[36] C.T. Shao, W.Z. Lang, X. Yan, Y.J. Guo, Catalytic performance of gallium oxide based-catalysts for the propane dehydrogenation reaction: effects of support and loading amount, RSC Adv. 7 (2017) 4710–4723, https://doi.org/10.1039/c6ra27204e.

[37] F. Jiang, L. Zeng, S. Li, G. Liu, S. Wang, J. Gong, Propane Dehydrogenation over Pt/TiO2 –Al2O3 Catalysts, ACS Catal. 5 (2015) 438–447, https://doi.org/10.1021/cs501279v.
[38] Y. Zhang, Y. Zhou, J. Shi, S. Zhou, X. Sheng, Z. Zhang, S. Xiang, Comparative study of bimetallic Pt-Sn catalysts supported on different supports for propane dehydrogenation, J. Mol. Catal. A Chem. 381 (2014) 138–147, https://doi.org/10.1016/j.molcata.2013.10.007.
[39] I. Lezcano-González, P. Cong, E. Campbell, M. Panchal, M. Agote-Arán, V. Celorrio, Q. He, R. Oord, B.M. Weckhuysen, A.M. Beale, Structure-activity relationships in highly active platinum-tin MFI-type zeolite catalysts for propane dehydrogenation, ChemCatChem 14 (2022) 1–7, https://doi.org/10.1002/cctc.202101828.
[40] Y. Yue, J. Fu, C. Wang, P. Yuan, X. Bao, Z. Xie, J.M. Basset, H. Zhu, Propane dehydrogenation catalyzed by single Lewis acid site in Sn-Beta zeolite, J. Catal. 395 (2021) 155–167, https://doi.org/10.1016/j.jcat.2020.12.019.
[41] B. Feng, Y.C. Wei, W.Y. Song, C.M. Xu, A review on the structure-performance relationship of the catalysts during propane dehydrogenation reaction, Pet. Sci. 19 (2022) 819–838, https://doi.org/10.1016/j.petsci.2021.09.015.
[42] Z. Feng, X. Liu, Y. Wang, C. Meng, Recent advances on gallium-modified zsm-5 for conversion of light hydrocarbons, Molecules 26 (2021) 2234, https://doi.org/10.3390/molecules26082234.
[43] S.W. Choi, W.G. Kim, J.S. So, J.S. Moore, Y. Liu, R.S. Dixit, J.G. Pendergast, C. Sievers, D.S. Sholl, S. Nair, C.W. Jones, Propane dehydrogenation catalyzed by gallosilicate MFI zeolites with perturbed acidity, J. Catal. 345 (2017) 113–123, https://doi.org/10.1016/j.jcat.2016.11.017.
[44] T. Waku, J.A. Biscardi, E. Iglesia, Active, selective, and stable Pt/Na-[Fe]ZSM5 catalyst for the dehydrogenation of light alkanes, Chem. Commun. 3 (2003) 1764–1765, https://doi.org/10.1039/b303506a.